R 76-11

AD

# GRAIN BOUNDARY DISLOCATIONS IN NONCUBIC CRYSTALS - II. THE GBD MODEL APPLIED TO GRAIN BOUNDARY FACETS IN $\langle 10\bar{1}0 \rangle$ TILT BOUNDARIES IN ZINC

GORDON A. BRUGGEMAN and GEORGE H. BISHOP, Jr.
MATERIALS SCIENCES DIVISION

March 1976



ARMY MATERIALS AND MECHANICS RESEARCH CENTER
Watertown, Massachusetts 02172

The findings in this report are not to be construed as an official Department of the Army position, unless so designated by other authorized documents.

Mention of any trade names or manufacturers in this report shall not be construed as advertising nor as an official indorsement or approval of such products or companies by the United States Government.

DISPOSITION INSTRUCTIONS

Destroy this report when it is no longer needed.
Do not return it to the originator.

UNCLASSIFIED

SECURITY CLASSIFICATION OF THIS PAGE (When Data Entered)

| REPORT DOCUMENTATION PAGE | | READ INSTRUCTIONS BEFORE COMPLETING FORM |
|---|---|---|
| 1. REPORT NUMBER<br>AMMRC TR 76-11 | 2. GOVT ACCESSION NO. | 3. RECIPIENT'S CATALOG NUMBER |
| 4. TITLE (and Subtitle)<br>GRAIN BOUNDARY DISLOCATIONS IN NONCUBIC CRYSTALS - II. THE GBD MODEL APPLIED TO GRAIN BOUNDARY FACETS IN <10$\bar{1}$0> TILT BOUNDARIES IN ZINC | | 5. TYPE OF REPORT & PERIOD COVERED<br>Final Report<br>6. PERFORMING ORG. REPORT NUMBER |
| 7. AUTHOR(s)<br>Gordon A. Bruggeman and George H. Bishop, Jr. | | 8. CONTRACT OR GRANT NUMBER(s) |
| 9. PERFORMING ORGANIZATION NAME AND ADDRESS<br>Army Materials and Mechanics Research Center<br>Watertown, Massachusetts 02172<br>DRXMR-D | | 10. PROGRAM ELEMENT, PROJECT, TASK AREA & WORK UNIT NUMBERS<br>D/A Project: 1T161102B32A<br>AMCMS Code: 611102.11.855<br>Agency Accession: DA 0D4767 |
| 11. CONTROLLING OFFICE NAME AND ADDRESS<br>U. S. Army Materiel Development and Readiness Command, Alexandria, Virgina 22333 | | 12. REPORT DATE<br>March 1976<br>13. NUMBER OF PAGES<br>21 |
| 14. MONITORING AGENCY NAME & ADDRESS(if different from Controlling Office) | | 15. SECURITY CLASS. (of this report)<br>Unclassified<br>15a. DECLASSIFICATION/DOWNGRADING SCHEDULE |

16. DISTRIBUTION STATEMENT (of this Report)

Approved for public release; distribution unlimited.

17. DISTRIBUTION STATEMENT (of the abstract entered in Block 20, if different from Report)

18. SUPPLEMENTARY NOTES

19. KEY WORDS (Continue on reverse side if necessary and identify by block number)

| | | |
|---|---|---|
| Grain boundaries | Topology | Crystal defects |
| Crystallography | Zinc | Models |
| Dislocations | Interfaces | Crystal structure |

20. ABSTRACT (Continue on reverse side if necessary and identify by block number)

(SEE REVERSE SIDE)

DD FORM 1 JAN 73 1473 EDITION OF 1 NOV 65 IS OBSOLETE

UNCLASSIFIED

SECURITY CLASSIFICATION OF THIS PAGE (When Data Entered)

Block No. 20

ABSTRACT

Observations of faceting of <10$\bar{1}$0> tilt grain boundaries in zinc and a coincidence structural unit model were reported in earlier papers. The facet inclinations were found to be monotonic functions of boundary misorientation in certain misorientation ranges. In this paper, the grain boundary dislocation (GBD) model developed earlier is used to describe the structure of these faceted boundaries. The model, which assumes the Burgers vectors of the GBD's to be lattice vectors of the complete-pattern-shift or DSC lattice derived from near-coincidence arrays in hcp crystals, is able to account for the experimentally observed changes in boundary inclination with misorientation. Observed facet morphologies are obtained with only certain GBD's, the core structures of which are shown to be equivalent to the structural units in the previously suggested structural unit model. Thus, the application of the GBD model to more general boundaries in noncubic crystals is illustrated, and thereby, the general equivalence of the GBD and coincidence structural unit models is clearly demonstrated.

CONTENTS

## INTRODUCTION

Grain boundaries deviating slightly from coincidence misorientations in cubic crystals have been observed, by transmission electron microscopy, to contain a network of grain boundary dislocations (GBD's) having Burgers vectors equal to lattice vectors of the "complete-pattern-shift" lattice or DSC lattice appropriate for that particular coincidence relationship.[1-7] These direct observations have supported the view that the structure of off-coincidence boundaries will consist predominantly of areas having the structure of the exact coincidence boundary separated from one another by intrinsic grain boundary defects, namely the GBD's. Unfortunately, verification of such predictions by direct observation are difficult, since the usual small size of the predicted Burgers vectors and their close spacing make their resolution by transmission microscopy unlikely in the great majority of instances.[8,9] Indeed, the GBD model thus formulated has received direct confirmation in relatively few instances, and these have almost exclusively been in cubic crystals. With the exception of a recent paper by Loberg and Smith,[10] grain boundary dislocations in hexagonal-close-packed (hcp) metals have not been treated.

In the previous paper (Reference 11, hereafter referred to as Part I), it was shown that as the grain boundary seeks its lowest energy, the presence of GBD's in certain tilt boundaries can produce a systematic and uniquely defined change in the boundary inclination as the misorientation across the boundary varies. Thus by experimentally observing the misorientation dependence of the low-energy boundary inclination, one can infer what the dislocation structure of that boundary must in fact be in order to have produced such a relationship between inclination and misorientation. Although the GBD's are not directly observed or their Burgers vectors directly identified by this means, nevertheless evidence of their presence, their nature, and their distribution is provided.

In an earlier study[12] zinc bicrystals were grown from the melt, such that a $<10\bar{1}0>$ tilt grain boundary separated the two crystals. Although the seed crystals


1. SCHOBER, T., and BALLUFFI, R. W. *Quantitative Observation of Misfit Dislocation Arrays in Low and High-Angle Twist Grain Boundaries.* Phil. Mag., v. 21, 1970, p. 109-123.
2. SCHOBER, T. *Observation of Misfit Dislocation Arrays in High Angle (110) Twist Grain Boundaries in Gold.* Phil. Mag., v. 22, 1970, p. 1063-1068.
3. SCHOBER, T., and BALLUFFI, R. W. *Extraneous Grain Boundary Dislocations in Low and High Angle (001) Twist Boundaries in Gold.* Phil. Mag., v. 24, 1971, p. 165-180.
4. SCHOBER, T., and BALLUFFI, R. W. *Dislocations in Symmetric High Angle [001] Tilt Boundaries in Gold.* Phys. Stat. Sol. (b), v. 44, 1971, p. 115-126.
5. SCHOBER, T., and WARRINGTON, D. H. *Extraneous Grain Boundary Dislocations in High Angle (110) Twist Boundaries in Gold.* Phys. Stat. Sol. (a), v. 6, 1971, p. 103-110.
6. BALLUFFI, R. W., KOMEN, Y., and SCHOBER, T. *Electron Microscope Studies of Grain Boundary Dislocation Behavior.* Surface Science, v. 31, 1972, p. 68-103.
7. BOLLMANN, W. *Crystal Defects and Crystalline Interfaces.* Springer-Verlag, 1970.
8. BALLUFFI, R. W., WOOLHOUSE, G. R., and KOMEN, Y. *On Grain Boundary Dislocation Contrast in the Electron Microscope* in The Nature and Behavior of Grain Boundaries. H. Hu, ed., Plenum Press, 1972, p. 41.
9. BALLUFFI, R. W., and TAN, T. Y. *Comments on the Range of Applicability of the Grain Boundary (Secondary) Dislocation Model to High Angle Grain Boundaries.* Scripta Met., v. 6, 1972, p. 1033-1040.
10. LOBERG, B., and SMITH, D. A. *Periodic Structures and Grain Boundaries in Magnesium.* J. Microscopy, v. 102, 1974, p. 317-322.
11. BRUGGEMAN, G. A., and BISHOP, G. H. *Grain Boundary Dislocations in Noncubic Crystals - I. The Model.* Army Materials and Mechanics Research Center, AMMRC TR 76-6, March 1976.
12. BISHOP, G. H., HARTT, W. H., and BRUGGEMAN, G. A. *Grain Boundary Faceting of $<10\bar{1}0>$ Tilt Boundaries in Zinc.* Acta Met., v. 19, 1971, p. 37-47.

were oriented so as to cause the macroscopic inclination of the boundary to be symmetric, the boundary was observed to develop distinct asymmetric facets which were identified as low-energy asymmetric <10$\bar{1}$0> tilt boundaries. The inclination of the facets relative to the symmetric inclination was observed to vary systematically with the misorientation.

This paper applies the GBD model developed in Part I to an analysis of these asymmetric <10$\bar{1}$0> tilt boundaries formed by grain boundary faceting in zinc. In the process low-energy coincidence patterns are identified along with their corresponding DSC lattices for boundaries in the misorientation range $30° < \theta < 37.25°$ and in the range $49.6° < \theta < 56.6°$. Resolution of the postulated GBD networks into a pattern-preserving array and a misfit array is made, as discussed in Part I. Observed facet morphologies are obtained with only certain GBD's, thereby identifying these as the intrinsic pattern-preserving defects in these particular asymmetric tilt boundaries. Comparisons are made with the coincidence structural unit model used earlier by the present authors to successfully describe these same faceted grain boundaries (Reference 13, hereafter referred to as HBB). The limited microscopic equivalence of the GBD model and the structural unit model, until now demonstrated only in the case of symmetric tilt boundaries in cubic crystals,[14,15] is thus shown to extend to more general grain boundaries in noncubic crystals. This fact is used to provide additional insight into the nature of the grain boundary dislocation arrays to be found in general low-energy boundaries.

## COINCIDENCE PATTERNS IN HCP CRYSTALS

Although exact coincidence-site lattices (CSL's) will exist in hcp crystals only when $(c/a)^2$ is a rational number (except for rotations about the c-axis), it has been possible to identify several near-CSL's in the hexagonal metals for which $(c/a)^2$ is irrational.[16] Those near-CSL's formed by rotations about <10$\bar{1}$0> will contribute the potential low-energy coincidence patterns that are preserved in the <10$\bar{1}$0> tilt boundaries of interest here.

When the CSL is exact, all of the two-dimensional coincidence patterns characteristic of coincidence grain boundaries of various inclinations are identified with a single misorientation (the coincidence misorientation, call it $\theta_o$). On the other hand, the two-dimensional coincidence patterns are less well defined in the near-coincidence case. Indeed, under the best of circumstances, only two of the coincidence patterns associated with a given near-CSL can be brought into exact coincidence, and these at two slightly different values of the misorientation, $\theta_1$ and $\theta_2$. (For <10$\bar{1}$0> rotations these are the two symmetric tilt boundaries, one at each of these two misorientations.) All other two-dimensional coincidence patterns are never exact, regardless of misorientation, and contain a residual shear distortion as discussed in Part I.

13. HARTT, W. H., BISHOP, G. H., and BRUGGEMAN, G. A. *Grain Boundary Faceting of <10$\bar{1}$0> Tilt Boundaries in Zinc - Part II.* Acta Met., v. 22, 1974, p. 971-983.
14. BISHOP, G. H., and CHALMERS, B. *A Coincidence-Ledge-Dislocation Description of Grain Boundaries.* Scripta Met., v. 2, 1968, p. 133-140.
15. BISHOP, G. H., and CHALMERS, B. *Dislocation Structure and Contrast in High-Angle Grain Boundaries.* Phil. Mag., v. 24, 1971, p. 515-526.
16. BRUGGEMAN, G. A., BISHOP, G. H., and HARTT, W. H. *Coincidence and Near-Coincidence Grain Boundaries in HCP Metals* in The Nature and Behavior of Grain Boundaries. H. Hu, ed., Plenum Press, 1972, p. 83.

Two-dimensional near-coincidence patterns can be locally constrained to conform to exact coincidence patterns by the introduction of suitable GBD's into the interface. In the exact coincidence case, GBD's are needed whenever there is a slight change in misorientation which destroys the long-range exact coincidence pattern. In the near-coincidence case, either the crystallography, which obviates exact coincidence, or a change in misorientation, or both may require the introduction of GBD's. As the difference between the two characteristic misorientations $\theta_1$ and $\theta_2$ increases, the crystallography becomes less and less conducive to the establishment of the coincidence pattern in a generally inclined grain boundary, i.e., the shear distortions become more severe. Thus, $|\theta_1 - \theta_2|$ is a measure of the shear distortions associated with the coincidence patterns of a particular near-CSL, and is indicative of the complexity of the dislocation array that must be involved if those patterns are to be preserved in the grain boundary structure.

Even though only near-CSL's occur at the c/a ratios of real hexagonal metals, there will be slightly different values of c/a for which each CSL is exact. Using the notation of Reference 16, the rotation angle and the idealized c/a ratio at which the various <10$\bar{1}$0> near-CSL's become exact CSL's are plotted in Figure 1. The extent to which the c/a ratio for exact coincidence deviates from the actual c/a ratio is related to the value $|\theta_1 - \theta_2|$, and so further reflects the shear distortions associated with near-coincidence in grain boundaries in the real crystal.*

As discussed in Part I, the low-energy coincidence patterns that are preserved in the boundary are exact coincidence patterns, i.e., they are the patterns defined by the exact CSL's. Since the exact CSL's exist only at well-defined values of c/a, the DSC lattices presenting the related pattern-preserving displacements can, in a strict sense, be identified only at these c/a values. The unit vectors of the exact DSC lattice, once identified at the idealized c/a,

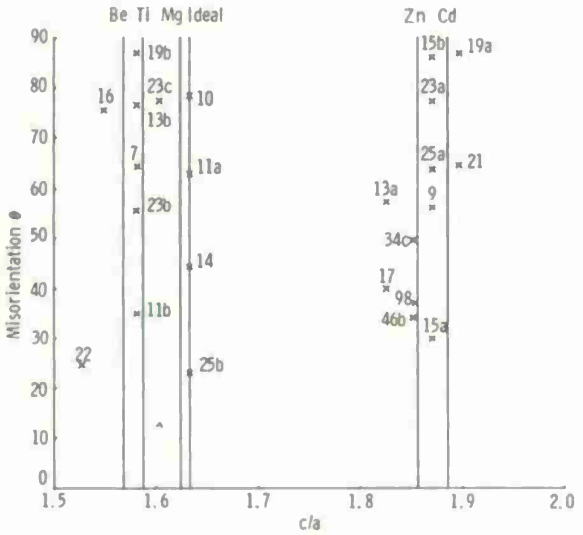


Figure 1. Various coincidence-site lattices for hcp crystals formed by misorientations about <10$\bar{1}$0>. The relative crystal misorientation producing each CSL is plotted at the value of c/a at which each is exactly coincident. The coincidence ratio $\Sigma$ is indicated for each CSL, following the notation in Reference 16.

*Figure 1 is drawn for room temperature values of c/a. As the c/a ratio changes with temperature or alloying, or both, the deviation from a given coincidence pattern will change. Thus the number and the type of GBD's may change if the shift in c/a moves the system further from one and closer to another CSL. This effect does not occur in cubic crystals.

however, are also the unit vectors of a modified DSC lattice in the real crystal. This modified DSC lattice is a slightly distorted version of the exact DSC lattice, and defines the equivalent pattern-preserving displacements in the real crystal. The unit vectors of the modified DSC lattice have the same indices as those of the exact DSC lattice, but differ very slightly in magnitude and direction due to the difference in c/a, although to the casual observer the exact and modified DSC lattices are indistinguishable.

## THE GBD MODEL OF BOUNDARY FACETS

It was shown in Part I that the shifting of the low-energy coincidence pattern caused by the displacement fields of the GBD's of the pattern-preserving dislocation array produced a systematic change in boundary inclination $\alpha$ with changing misorientation $\theta$ in tilt boundaries. It was shown that

$$\Delta\theta = \frac{b_p \cos(\gamma-\alpha)\, \sin(\alpha-\alpha_o)\, \cos\beta}{L\, \cos(\beta-\alpha)\, \cos\alpha} \qquad (1)$$

where the various parameters have the meaning given in Part I (cf. Figure 7 of Part I). Of the numerous combinations of low-energy coincidence patterns, lattice displacements, and pattern shifts that are possible, the analysis which follows concentrates on those which have significance to the experimental observations of grain boundary faceting in zinc. Specifically, $<10\bar{1}0>$ tilt boundaries are described whose inclinations, measured relative to the symmetric inclination, increase as the misorientation $\theta$ increases from 30° to 37.5°, and decrease as the misorientation increases from 49.6° to 56.6°.

The structural unit model for grain boundary structure draws upon boundary segments of near-coincidence boundaries passing through the near-CSL's as sources for probable low-energy structural units. In particular, the structural units used in the previous analysis of faceting of $<10\bar{1}0>$ tilt boundaries in zinc by HBB were based upon the $\Sigma$ = 15, 46, and 98 near-CSL's for boundaries in the misorientation range $30° < \theta < 37.5°$, and on the $\Sigma$ = 9 and 34 near-CSL's for boundaries in the misorientation range $49.6° < \theta < 56.6°$. By analogy, the present GBD description of faceted $<10\bar{1}0>$ tilt boundaries will draw upon the coincidence patterns associated with these same near-CSL's as sources of probable low-energy patterns to be preserved within these same misorientation ranges.

Figures 2 through 5 present one layer of the $\Sigma$ = 15, 46, 34, and 9 near-CSL's and their associated DSC lattices, each showing a boundary characterized by a probable low-energy coincidence pattern.* Figures 2b, 3b, 4b, and 5b show the unit cells of the DSC lattices related to the near-CSL's of Figures 2a, 3a, 4a, and 5a. The relative positions of the $\{10\bar{1}0\}$ planes of the four-layered $\{10\bar{1}0\}$ stacking sequence are indicated. Also shown is an expanded section through each DSC lattice normal to the $<10\bar{1}0>$ rotation axis, defining the pertinent DSC unit vectors. The unit vectors of the DSC lattices corresponding to the $\Sigma$ = 9, 15, 34,

*Previous experimental observations (Reference 12) provide strong evidence that these are indeed low-energy configurations.

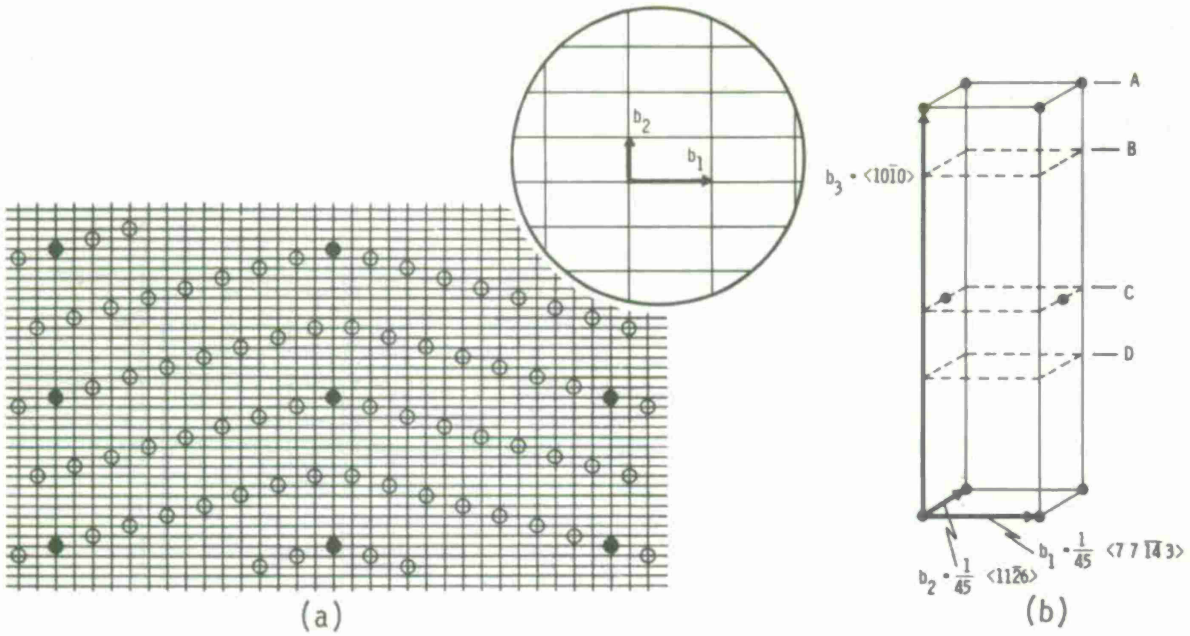


Figure 2. (a) A symmetric tilt boundary passing through the $\Sigma = 15$ near-coincidence-site lattice formed by a misorientation of 30.15° about $\langle 10\bar{1}0 \rangle$ in zinc. The filled circles are coincidence lattice sites. The lines correspond to one layer of the related DSC lattice. An expanded view of the DSC lattice, presenting the unit vectors, is also shown. (b) The unit cell of the $\Sigma = 15$ DSC lattice. The relative positions of the four layers of the $\langle 10\bar{1}0 \rangle$ stacking sequence are indicated at A, B, C, and D.

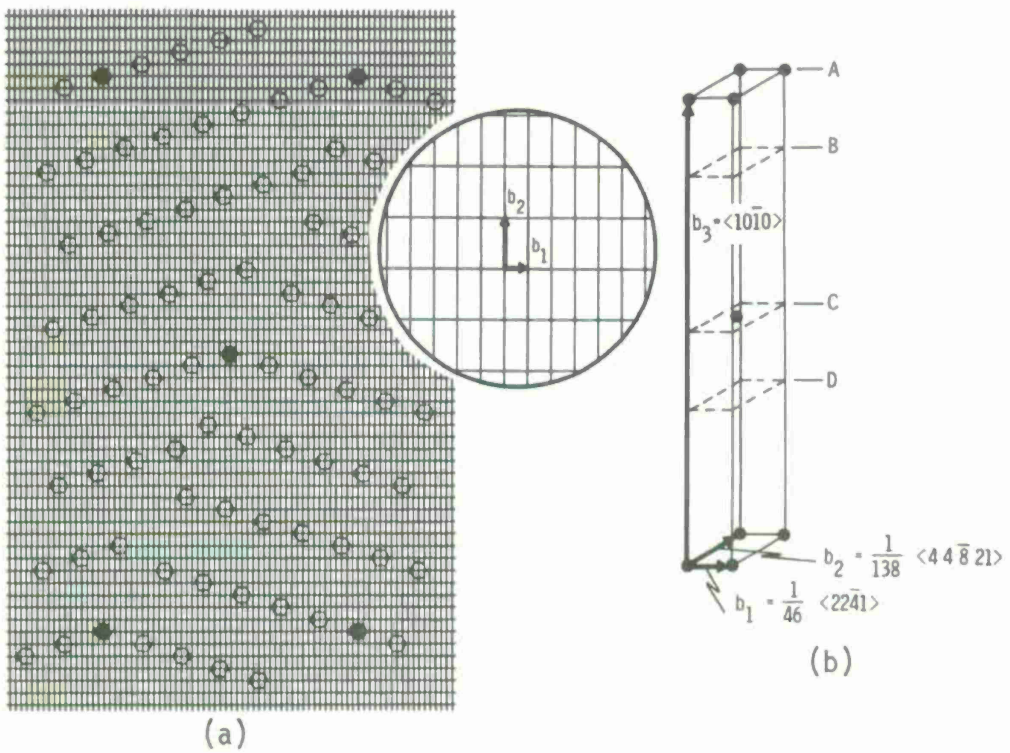


Figure 3. (a) An asymmetric tilt boundary passing through the $\Sigma = 46$ near-coincidence-site lattice formed by a misorientation of 34.25° about $\langle 10\bar{1}0 \rangle$ in zinc. The filled circles are coincidence lattice sites. The lines correspond to one layer of the related DSC lattice. An expanded view of the DSC lattice, presenting the unit vectors, is also shown. (b) The unit cell of the $\Sigma = 46$ DSC lattice.

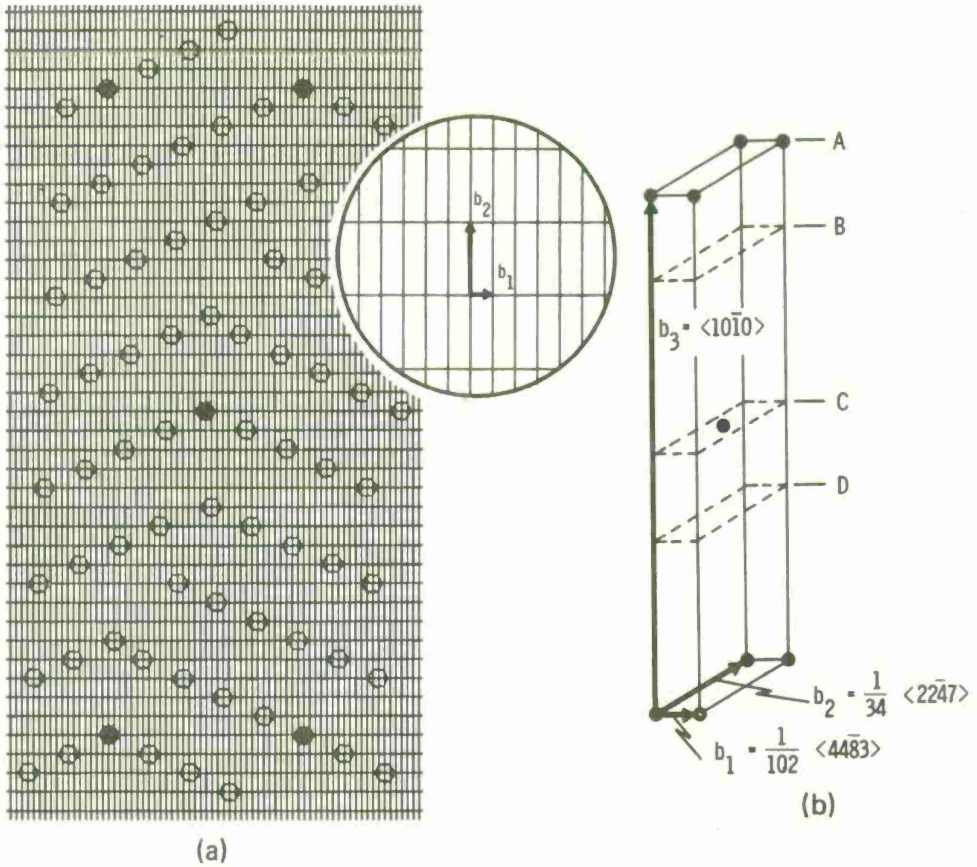


Figure 4. (a) An asymmetric tilt boundary passing through the $\Sigma = 34$ near-coincidence-site lattice formed by a misorientation of 49.59° about $<10\bar{1}0>$ in zinc. The filled circles are coincidence lattice sites. The lines correspond to one layer of the related DSC lattice. An expanded view of the DSC lattice, presenting the unit vectors, is also shown. (b) The unit cell of the $\Sigma = 34$ DSC lattice.

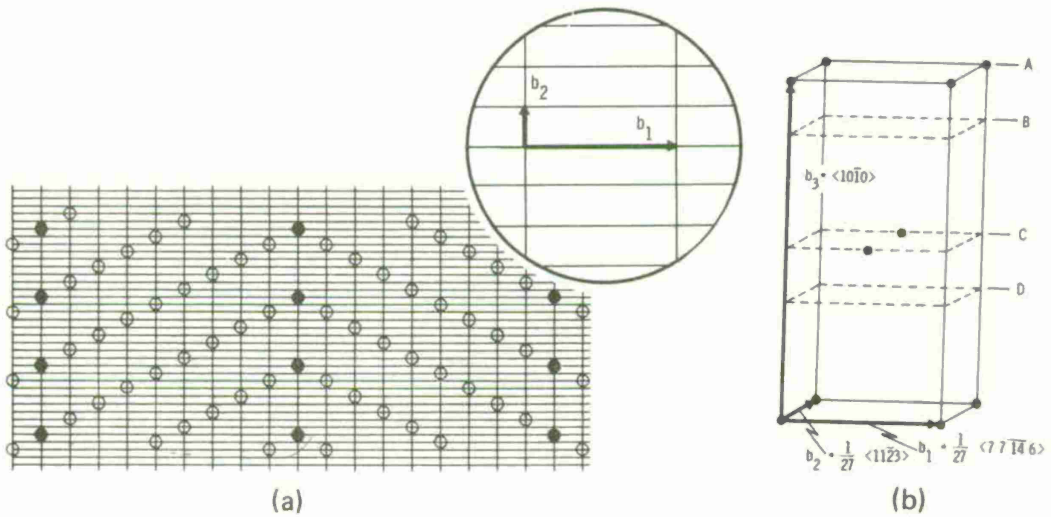


Figure 5. (a) A symmetric tilt boundary passing through the $\Sigma = 9$ near-coincidence-site lattice formed by a misorientation of 56.62° about $<10\bar{1}0>$ in zinc. The filled circles are coincidence lattice sites. The lines correspond to one layer of the related DSC lattice, an expanded view of which is also shown. (b) The unit cell of the $\Sigma = 9$ DSC lattice.

and 46 near-CSL's are also presented in Table 1. The characteristic misorientations $\theta_1$ and $\theta_2$ are taken such that at $\theta_1$ coincidence is exact in the symmetric tilt boundary parallel to $b_2$ (vertical), and at $\theta_2$ coincidence is exact in the symmetric tilt boundary parallel to $b_1$ (horizontal). Values of $\theta_1$ and $\theta_2$ pertinent to zinc (c/a = 1.8563) are listed in Table 1. The tilt boundary segments shown in Figures 2 through 5 are assumed to represent the low-energy coincidence patterns preserved in the observed faceted grain boundaries in zinc. Both experimentally and in the analysis, the boundary inclination $\alpha$ is measured relative to the symmetric inclination parallel to $b_2$, which in every case is vertical. The asymmetric inclination is taken to be that which is rotated clockwise about $\langle 10\bar{1}0 \rangle$ from the symmetric inclination, although, by symmetry, the counter-clockwise rotation will lead to an equivalent structure.

Table 1. UNIT VECTORS OF DSC LATTICES ASSOCIATED WITH SOME COINCIDENCE PATTERNS IN ZINC FORMED BY ROTATIONS ABOUT $\langle 10\bar{1}0 \rangle$

| $\Sigma$ | $\theta_1$ | $b_1$ | $\lvert b_1 \rvert$ | $\theta_2$ | $b_2$ | $\lvert b_2 \rvert$ |
|---|---|---|---|---|---|---|
| 9 | 56.62° | $1/27 \langle 7\ 7\ \bar{14}\ 6 \rangle$ | 0.8804a | 55.88° | $1/27 \langle 11\bar{2}3 \rangle$ | 0.2343a |
| 15 | 30.15° | $1/45 \langle 7\ 7\ \bar{14}\ 3 \rangle$ | 0.4828a | 29.70° | $1/45 \langle 11\bar{2}6 \rangle$ | 0.2563a |
| 34 | 49.57° | $1/102 \langle 44\bar{8}3 \rangle$ | 0.1297a | 49.79° | $1/34 \langle 22\bar{4}7 \rangle$ | 0.4210a |
| 46 | 34.22° | $1/46 \langle 22\bar{4}1 \rangle$ | 0.1365a | 34.38° | $1/138 \langle 4\ 4\ \bar{8}\ 21 \rangle$ | 0.2956a |

The boundary shown passing through the $\Sigma = 15$ near-CSL in Figure 2a is the $\{11\bar{2}1\}$ symmetric twin interface, one repeat segment of which was referred to by HBB as the symmetric structural unit $S_1$ occurring at the characteristic misorientation of 30.15° (equal to $\theta_1$) in zinc. The asymmetric boundary passing through the $\Sigma = 46$ near-CSL in Figure 3a is made up, in the structural unit view of HBB, of asymmetric structural units designated $A_1$, occurring at the characteristic misorientation of 34.25°.* Similarly, the asymmetric boundary passing through the $\Sigma = 34$ near-CSL in Figure 4a contains asymmetric structural units previously designated $A_1'$, occurring at the characteristic misorientation of 49.62° in zinc.* Finally, the boundary shown passing through the $\Sigma = 9$ near-CSL in Figure 5a is the $\{11\bar{2}2\}$ symmetric twin interface, one repeat segment of which was designated by HBB as the $S_2$ symmetric structural unit, occurring at the characteristic misorientation of 56.62° (equal to $\theta_1$) in zinc.

Having identified or postulated a low-energy coincidence pattern to be preserved in the boundary and its associated DSC lattice, possible Burgers vectors for GBD's of the pattern-preserving array can be selected and the corresponding boundary offset L determined graphically from observed pattern shifts produced by the pertinent lattice displacements in crystallographic overlays. For each possible GBD, the theoretical relationship between $\Delta\theta$ and $\alpha$ can be determined from Equation 1 and comparison made with experimentally measured values of these quantities.

Table 2 presents some of the possible Burgers vectors, $b_p$, of the pattern-preserving GBD's related to the preservation of the $\Sigma = 15$ symmetric coincidence pattern of Figure 2, along with the values for $\gamma$ and the pattern shift distance L.

*This is one of the special boundary misorientations and inclinations discussed in Part I for which $\theta_1 < \theta < \theta_2$ and $\alpha - \beta = 90°$, leading to the requirement for an array of misfit dislocations in the boundary but no pattern-preserving array.

Table 2. BURGERS VECTORS CORRESPONDING TO PATTERN-PRESERVING DISPLACEMENTS IN THE MISORIENTATION RANGE $30.1° < \theta < 37.5°$

| | b | \|b\| | γ | L | $(d\alpha/d\theta)_{\alpha\to\alpha_0}$ |
|---|---|---|---|---|---|
| Σ = 15 Coincidence Pattern (Figure 2) $\theta_1 = 30.15°$ $\alpha_0 = 0°$ | $2b_1$ | 0.966a | 0 | 0 | 0 |
| | $b_1$ | 0.483a | 0 | 15/2 $b_1$=3.621a | 7.50 |
| | $b_1$ | 0.483a | 0 | 0* | 0 |
| | $b_1-b_2$ | 0.547a | 27.96° | 13/2 $b_1$=3.138a | 6.49 |
| | $b_1+b_2$ | 0.547a | -27.96° | $b_1$=0.483a* | 1.00 |
| Σ = 46 Coincidence Pattern (Figure 3) $\theta_1 = 34.22°$ $\alpha_0 = 24.79°$ | $-2b_1$ | 0.273a | 0 | $-13b_2\sin\alpha_0$=-1.611a | 6.50 |
| | $3b_1-b_2$ | 0.505a | 35.82 | 39/2 $b_1\cos\alpha_0$- 7/2 $b_2\sin\alpha_0$=1.983a | 4.00 |

*Pattern is also shifted parallel to the $\langle 10\bar{1}0\rangle$ tilt axis.

(The dislocations of the misfit array will be discussed later.) Figures 6 through 8 illustrate three examples of dislocation core structures taken from the table. In each case, the GBD Burgers vector is made evident by the closure failure of the Burgers circuit[17] drawn in the Σ = 15 DSC lattice. Figure 6 shows a boundary with a misorientation slightly greater than 30.15°, containing a dislocation with a Burgers vector equal to $2b_1$. (Here $b_1$ and $b_2$ refer to unit vectors of the Σ = 15 DSC lattice.) In this case, the boundary has remained in the symmetric inclination since the pattern has only shifted in the plane of the boundary and not normal to it. Figure 7 illustrates a GBD with Burgers vector $b_1$, where there has been a component of the pattern shift parallel to the $\langle 10\bar{1}0\rangle$ rotation axis, causing the coincidence pattern to be reestablished in a different $\{10\bar{1}0\}$ layer of the four-layered $\{10\bar{1}0\}$ stacking sequence (the layer designated B in Figures 2 through 5). Several other examples of this type have been cited in the table (those marked by an asterisk), in which the pattern is shifted to another $\{10\bar{1}0\}$ plane. Although GBD's with such Burgers vectors may play a significant role in the structure of some boundaries, they do not appear to do so in the experimentally observed boundaries of interest here; therefore, they will not be discussed further. Figure 8 illustrates a boundary with a misorientation slightly greater than 30.15°, where the GBD with Burgers vector $(b_1-b_2)$ has caused a pattern shift leading to an alteration of the boundary inclination. The more closely spaced these latter GBD's are, the greater becomes the deviation of the boundary misorientation from that of the Σ = 15 coincidence pattern, and also the more the boundary inclination deviates from that of the symmetric inclination.

Table 2 also presents some Burgers vectors of GBD's capable of preserving the Σ = 46 asymmetric coincidence pattern of Figure 3. (In this case, $b_1$ and $b_2$ will refer to unit vectors of the Σ = 46 DSC lattice.) A Burgers vector of $-2b_1$ allows the boundary misorientation to be decreased while rotating the boundary inclination closer to the symmetric inclination. This GBD is shown in Figure 9. Again, the closure failure in the Burgers circuit, this time drawn in the Σ = 46 DSC lattice, indicates the GBD Burgers vector. Also, a Burgers vector of $(3b_1-b_2)$ will increase θ while rotating the boundary inclination further away from the symmetric inclination.

17. HIRTH, J. P., and BALLUFFI, R. W. *On Grain Boundary Dislocations and Ledges.* Acta Met., v. 21, 1973, p. 929-942.

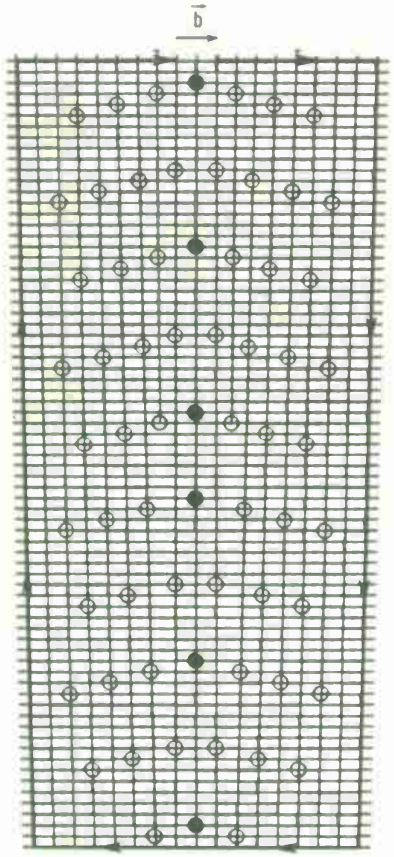


Figure 6. A schematic representation of a GBD with Burgers vector $2b_1$ which preserves the symmetric $\Sigma = 15$ coincidence pattern on both sides of the dislocation. This and subsequent figures illustrating various GBD's are schematic in the sense that the elastic strain field of the dislocation is not represented correctly. The circles represent lattice sites but not necessarily atom positions.

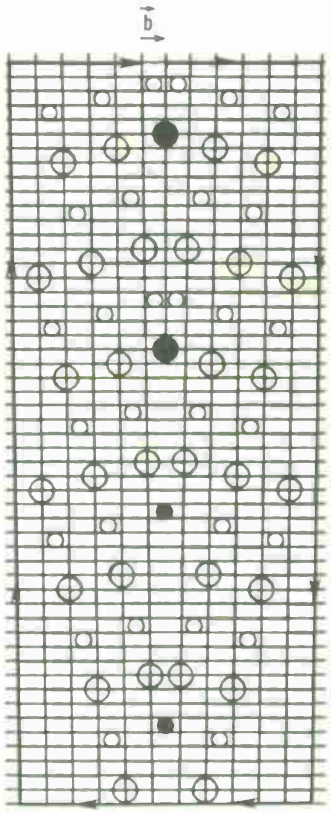


Figure 7. A schematic representation of a GBD with Burgers vector $b_1$ which preserves the symmetric $\Sigma = 15$ coincidence pattern while maintaining the boundary in the symmetric inclination. The large circles are sites in layer A, the small circles are sites in layer B (see Figure 2b).

The changes in boundary inclination produced by the introduction of the above GBD's into the structure of boundaries in the misorientation range $30.1^\circ < \theta < 37.5^\circ$ are plotted in Figure 10, based upon the relationship derived in Equation 1. The three open circles in Figure 10 represent the inclinations and misorientations of the low-energy coincidence patterns; the filled circles are experimentally observed boundary inclinations in as-grown zinc bi- and tri-crystals, the same data as presented by HBB. The lines emanating from the open circle at $\theta = 30.15^\circ$ represent boundaries in which the $\Sigma = 15$ coincidence pattern is preserved by the presence of the indicated GBD's in the boundary structure. The lines emanating from the open circle at $\theta = 34.25^\circ$ represent boundaries in which the $\Sigma = 46$ asymmetric coincidence pattern is preserved.

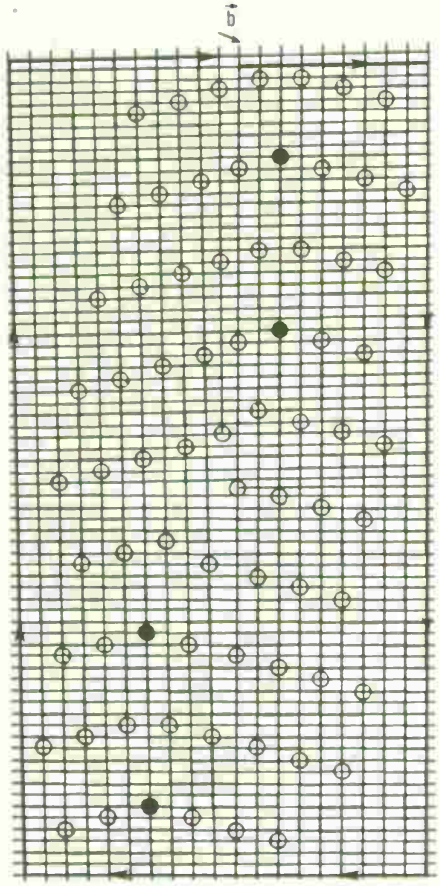

Figure 8. A schematic representation of a GBD with Burgers vector $(b_1-b_2)$ which preserves the symmetric $\Sigma = 15$ coincidence pattern while causing the boundary to become inclined relative to the symmetric inclination.

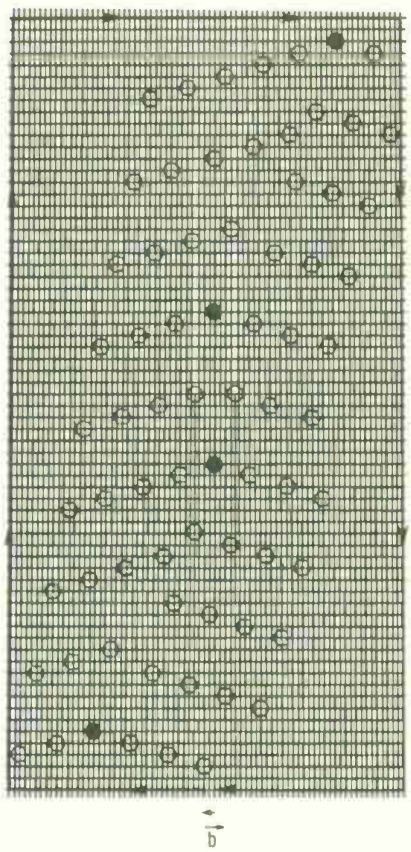

Figure 9. A schematic representation of a GBD with Burgers vector $-2b_1$ which preserves the asymmetric $\Sigma = 46$ coincidence pattern while causing the boundary inclination to be rotated closer to that of the symmetric inclination.

The experimental data indicate that the $\Sigma = 15$ symmetric coincidence pattern is preserved in faceted boundaries predominantly by GBD's with Burgers vectors of $(b_1-b_2)$, while the $\Sigma = 46$ asymmetric coincidence pattern is preserved in boundary facets at misorientations below 34.25° by GBD's with Burgers vectors of $-2b_1$ and above 34.25° by GBD's with Burgers vectors of $(3b_1-b_2)$. The spacing of these dislocations will decrease as the misorientation deviates more and more from the misorientation characteristic of the low-energy coincidence pattern.

Table 3 presents some Burgers vectors of the pattern-preserving GBD's which preserve the $\Sigma = 34$ asymmetric coincidence pattern and the $\Sigma = 9$ symmetric coincidence pattern of Figures 4 and 5. (Here, of course, $b_1$ and $b_2$ refer to unit vectors of the appropriate DSC lattice.) The GBD with Burgers vector $2b_1$ is shown in Figure 11 in a boundary with a misorientation slightly greater than 49.6°, in which the $\Sigma = 34$ asymmetric coincidence pattern is preserved. Here the GBD has caused the boundary inclination to be rotated nearer the symmetric inclination.

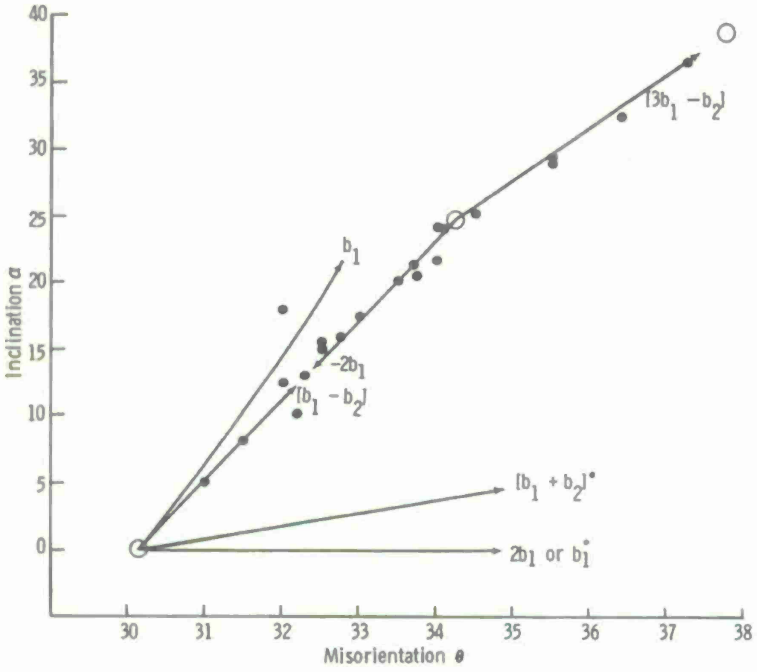


Figure 10. The boundary inclinations produced in boundaries of various dislocation structures plotted versus the boundary misorientation in the range $30.1^\circ < \theta < 37.5^\circ$. The open circles are the inclinations and misorientations of the designated coincidence patterns; the filled circles are actual experimental observations of faceted boundary inclinations. The arrows point away from the coincidence pattern being preserved by the GBD's with the indicated Burgers vectors.

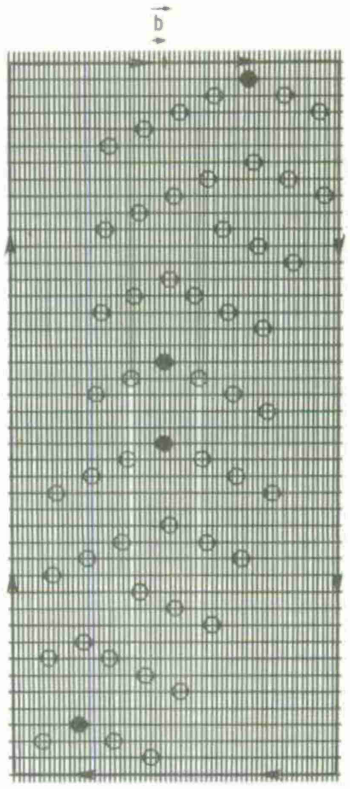


Figure 11. A schematic representation of a GBD with Burgers vector $2b_1$ which preserves the asymmetric $\Sigma = 34$ coincidence pattern while causing the boundary inclination to be rotated closer to that of the symmetric inclination.

Table 3. BURGERS VECTORS CORRESPONDING TO PATTERN-PRESERVING DISPLACEMENTS IN THE MISORIENTATION RANGE $49.6^\circ < \theta < 56.6^\circ$

| | b | \|b\| | γ | L | $(d\alpha/d\theta)_{\alpha\to\alpha_0}$ |
|---|---|---|---|---|---|
| $\Sigma = 34$ Coincidence Pattern (Figure 4) $\theta_1 = 49.57^\circ$ $\alpha_0 = 17.12^\circ$ | $2b_1$ | 0.259a | 0 | $5b_2 \sin\alpha_0 = 0.620a$ | -2.50 |
| $\Sigma = 9$ Coincidence Pattern (Figure 5) $\theta_1 = 56.62^\circ$ $\alpha_0 = 0^\circ$ | $-2b_1$ | 1.761a | 0 | 0 | 0 |
| | $-b_1$ | 0.880a | 0 | $9/2\ b_1 = 3.962a$ | -4.50 |
| | $-b_1$ | 0.880a | 0 | 0* | 0 |
| | $-b_1+b_2$ | 0.911a | 14.90° | $5/2\ b_1 = 2.201a$ | -2.50 |
| | $-b_1-b_2$ | 0.911a | -14.90° | $2b_1 = 1.761a$* | -0.94 |
| | $-b_1+2b_2$ | 0.997a | 28.03° | $1/2\ b_1 = 0.440a$ | -0.50 |
| | $-b_1-2b_2$ | 0.997a | -28.03° | $4b_1 = 3.522a$* | -4.00 |
| | $-b_1+3b_2$ | 1.127a | 38.60° | $3/2\ b_1 = 1.321a$ | -1.50 |
| | $-b_1-3b_2$ | 1.127a | -38.60° | $3b_1 = 2.641a$* | -3.00 |

*Pattern is also shifted parallel to the $\langle 10\bar{1}0\rangle$ tilt axis.

Figures 12 and 13 illustrate GBD's in boundaries in which the $\Sigma = 9$ coincidence pattern is preserved. The GBD with Burgers vector $-2b_1$ preserves the pattern in the boundary in the symmetric inclination (Figure 12). The GBD with Burgers vector $(-b_1+b_2)$ causes the boundary inclination to be rotated away from the symmetric inclination as the misorientation decreases (Figure 13). In each case, the Burgers circuit is shown drawn in the appropriate DSC lattice. Several other GBD's which cause the boundary to be inclined away from the symmetric inclination are presented in Table 3.

The changes in boundary inclination produced by the introduction of the above GBD's into the structures of boundaries in the misorientation range $49.6° < \theta < 56.6°$ are plotted in Figure 14. The two open circles represent the inclinations and misorientations of the low-energy coincidence patterns; the filled circles are experimentally observed boundary inclinations. The lines represent the relation in Equation 1, the line emanating from the open circle at $\theta = 49.6°$ representing boundaries in which the $\Sigma = 34$ asymmetric coincidence pattern is preserved, the lines emanating from the open circle at $\theta = 56.62°$ representing boundaries in which the $\Sigma = 9$ symmetric coincidence pattern is preserved. The experimental data points falling on or close to several of these lines would appear to indicate that several different dislocation structures have developed in the $<10\bar{1}0>$ tilt boundaries in this misorientation range.

The structural unit model of HBB previously described the structure of boundary facets formed in the misorientation range $30.15° < \theta < 34.25°$ as binary mixtures of symmetric structural units from the $\Sigma = 15$ near-CSL and asymmetric structural units from the $\Sigma = 46$ near-CSL, and so predicted that the boundary inclinations should lie along a line joining these two units on a plot of boundary inclination versus boundary misorientation as in Figure 10. The nearly linear relationship predicted by the structural unit model is precisely the relationship given by the GBD description when the $\Sigma = 15$ coincidence pattern is preserved by $(b_1-b_2)$ GBD's at the lower end of this misorientation range and the $\Sigma = 46$ coincidence pattern is preserved by $-2b_1$ GBD's at the higher end of the range. Similarly, above 34.25° the structural unit model described the facet structure as binary mixtures of the $\Sigma = 46$ asymmetric structural unit and the $\Sigma = 98$ asymmetric structural unit, and predicted that boundary inclinations intermediate between the inclinations of the component units would form. This also is precisely the prediction of the GBD model when the $\Sigma = 46$ coincidence pattern is preserved by $(3b_1-b_2)$ GBD's. The two descriptions are thus shown to be equivalent.

This equivalence is understood when one examines closely the core structures of the dislocations illustrated in Figures 8 and 9. The core structure of the dislocation in Figure 8, which preserves the $\Sigma = 15$ symmetric coincidence pattern, is simply a segment of the $\Sigma = 46$ asymmetric coincidence pattern of Figure 3. Conversely, the core structure of the dislocation in Figure 9, which preserves the $\Sigma = 46$ asymmetric coincidence pattern, is simply a segment of the $\Sigma = 15$ symmetric coincidence pattern of Figure 2. It thus appears that of the many possible GBD's with Burgers vectors capable of preserving the low-energy coincidence patterns, the ones that are most often selected are ones whose core structure most resembles another short period (and, therefore, low energy) coincidence pattern.

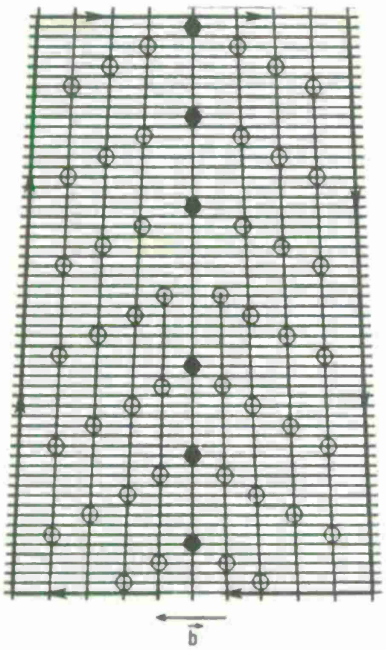


Figure 12. A schematic representation of a GBD with Burgers vector $-2b_1$ which preserves the symmetric $\Sigma = 9$ coincidence pattern while maintaining the boundary in the symmetric inclination.

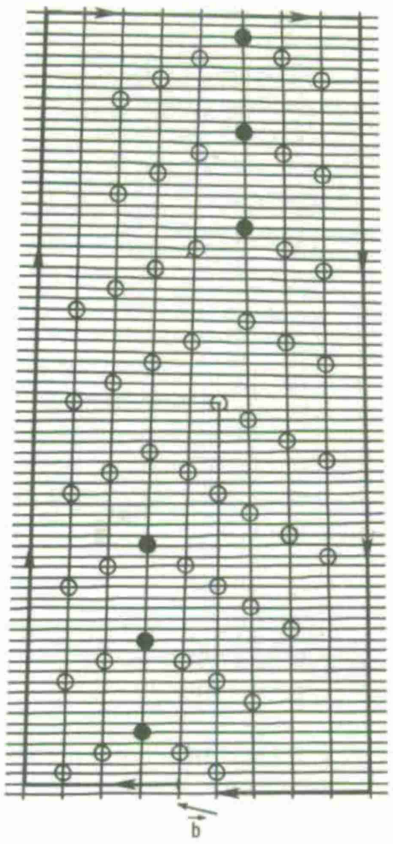


Figure 13. A schematic representation of a GBD with Burgers vector $(-b_1+b_2)$ which preserves the symmetric $\Sigma = 9$ coincidence pattern while causing the boundary to become inclined relative to the symmetric inclination.

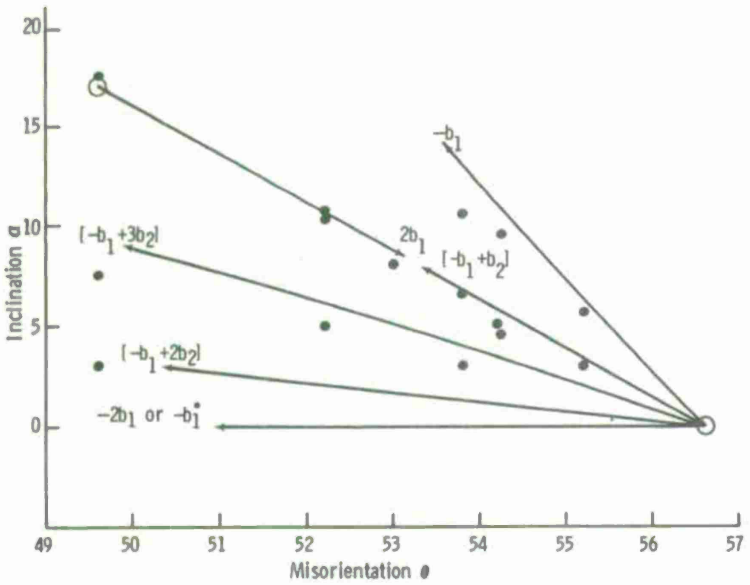


Figure 14. The boundary inclinations produced in boundaries of various dislocation structures plotted versus the boundary misorientation in the range $49.6° < \theta < 56.6°$. The open circles are the inclinations and misorientations of the designated coincidence patterns; the filled circles are actual experimental observations of faceted boundary inclinations. The arrows point away from the coincidence pattern being preserved by the GBD's with the indicated Burgers vectors.

This same equivalence of the structural unit and the GBD models is shown in the misorientation range $49.6° < \theta < 56.6°$. In this range, the structural unit model of HBB described faceted boundaries as binary mixtures of asymmetric structural units from the $\Sigma = 34$ near-CSL and symmetric structural units from the $\Sigma = 9$ near-CSL. Again, the predicted boundary inclinations are precisely those given by the GBD model when the $\Sigma = 34$ coincidence pattern is preserved by $2b_1$ GBD's at the lower end of the misorientation range, and the $\Sigma = 9$ coincidence pattern is preserved by $(-b_1+b_2)$ GBD's at the higher end of the range. It would appear from Figure 14, however, that some observed boundary facets may contain $-b_1$, $(-b_1+b_2)$, and $(-b_1+3b_2)$ GBD's all preserving the $\Sigma = 9$ symmetric coincidence pattern. The facet inclinations corresponding to these latter dislocation structures could not be explained satisfactorily by the structural unit model.

Referring to Figures 11 and 13, one can observe that the core structure of the $2b_1$ GBD preserving the $\Sigma = 34$ coincidence pattern is equivalent to the $\Sigma = 9$ symmetric structural unit, and that the core structure of the $(-b_1+b_2)$ GBD preserving the $\Sigma = 9$ coincidence pattern is equivalent to the $\Sigma = 34$ asymmetric structural unit. However, the preference for GBD's with core structures resembling other coincidence patterns is not as marked in this misorientation range, possibly because the coincidence patterns are not as distinctively low-energy as they were in the lower misorientation range. This view is supported by the fact that experimentally the boundary facets in the $49.6° < \theta < 56.6°$ misorientation range were not nearly as well developed or as sharply defined as were the facets in the $30.1° < \theta < 37.5°$ misorientation range. Nevertheless, the expectations for the development of boundary facets is probably greatest when the core structure of possible GBD's may be identified with short-period coincidence patterns such as these.

## THE MISFIT ARRAY

Thus far, the discussion has been directed toward the GBD's of the pattern-preserving array. The Burgers vectors of these pattern-preserving GBD's appear to be selected primarily on the basis that their core energy contribution to the total boundary energy is small (i.e., there is good atomic fit in the vicinity of the GBD). As a consequence, however, the Burgers vector of the pattern-preserving array does not bear the proper relationship to the boundary inclination that it must if there is to be no net grain boundary shear. In Part I it was pointed out that in crystal systems that can exhibit exact coincidence, the net Burgers vector will always be normal to the boundary plane in tilt boundaries. On the other hand, in crystal systems that exhibit only near-coincidence; the net Burgers vector is usually not normal to the boundary plane in tilt boundaries, but it does take on a uniquely defined orientation that depends upon boundary inclination and the characteristic misorientations, $\theta_1$ and $\theta_2$, of the near-CSL (cf. Figure 6c in Part I). Thus, in both cases, stability of the pattern-preserving array of GBD's relies upon an accompanying array of misfit dislocations to compensate the shear strain introduced by the former.

Figure 15a schematically presents the dislocation structure of the pattern-preserving array in boundaries of various misorientations. These resemble those arrays of pattern-preserving GBD's which most closely lead to the experimentally observed facet morphologies in zinc. Figure 15b presents in one typical case

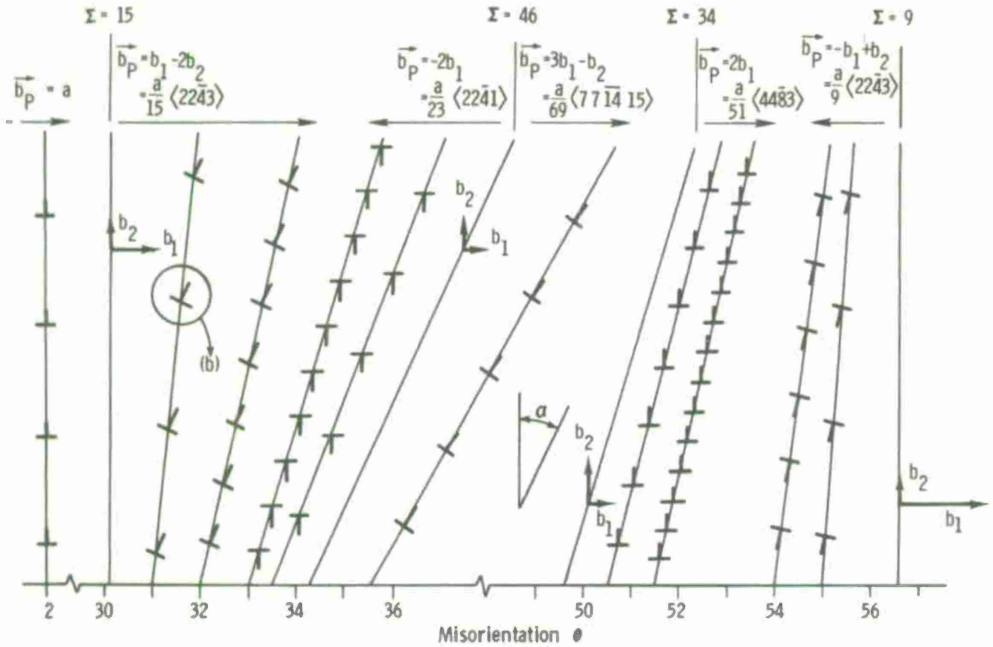


Figure 15a. A schematic representation of the dislocations of the pattern-preserving array in various <1010> tilt boundaries in zinc, illustrating the changing boundary inclination with dislocation structure. The boundary misorientation is given by the intercept of the boundary trace on the horizontal axis. The dislocation spacings have all been drawn to the same approximate scale as the spacing in the low-angle 2° tilt boundary.

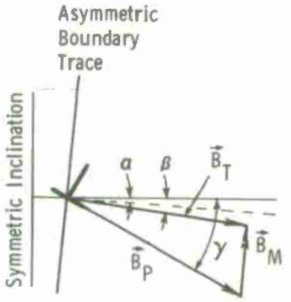


Figure 15b. The normalized total Burgers vector shown resolved into a normalized pattern-preserving Burgers vector component and a normalized misfit Burgers vector component. The example is taken from the boundary indicated in (a).

the normalized pattern-preserving Burgers vector in relation to the normalized total Burgers vector.* The required normalized misfit Burgers vector $B_M$ is the vector difference of these two. By calculating the magnitude of this vector difference for all pattern-preserving arrays as a function of misorientation, one obtains a measure of the boundary shear introduced by the pattern-preserving array in each case.

The magnitude of this boundary shear (or equivalently the strength of the normalized Burgers vector of the misfit array) is plotted in Figure 16 for the several possible pattern-preserving arrays considered earlier. The experimentally observed facet inclinations appear, in nearly every case, to be given by the pattern-preserving arrays requiring the smallest normalized misfit Burgers vectors. Thus, the boundary shear strain associated with the pattern-preserving array appears to be a second critical factor (along with dislocation core structure) which acts in the selection of the optimum Burgers vector for the pattern-preserving GBD's and hence of the resulting low-energy inclination for the boundary facets. Interestingly, the energy of the boundary facets is lower than that of the symmetric inclination for which no misfit array is ever necessary. The lower energy of the pattern-preserving GBD's that shift the boundary into the asymmetric inclination apparently mitigates the added energy contribution of the misfit array, allowing the energy of the facet inclination to remain low relative to that of the symmetric inclination at off-coincidence misorientations.

*The term "normalized Burgers vector" denotes the Burgers vector per unit length of boundary, as defined in Part I.

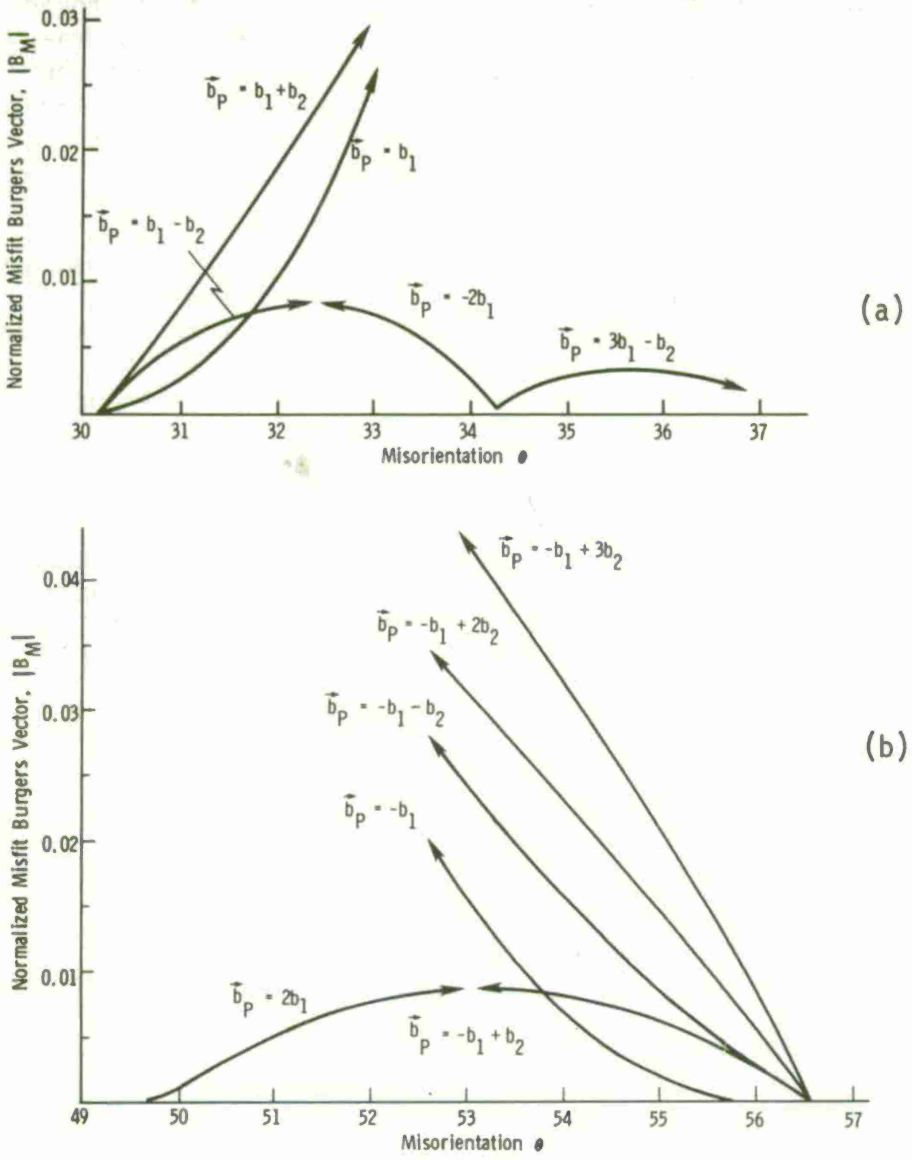


Figure 16. The magnitude of the normalized Burgers vector of the misfit dislocation array required to stabilize pattern-preserving arrays having various Burgers vectors, (a) in the misorientation range $30° < \theta < 37.5°$ and (b) misorientation range $49.6° < \theta < 56.6°$.

## SUMMARY

The grain boundary dislocation model for boundary structure in noncubic crystals has been applied to an analysis of experimentally observed grain boundary facets in <10$\bar{1}$0> tilt boundaries in zinc. Various coincidence patterns and their corresponding DSC lattices, pertinent to these particular asymmetric tilt boundaries, are identified and compared with the structural units proposed earlier by HBB in their coincidence structural unit model for these same boundaries. Various possible pattern-preserving GBD's, with Burgers vectors given by vectors of the appropriate DSC lattice, are considered and the approximate atomic configuration in the vicinity of the GBD depicted.

The misorientation dependence of the boundary inclination is calculated for several possible GBD's and compared with the experimentally observed misorientation dependence. It is shown that only certain GBD's are capable of explaining the

experimental observations, identifying these as the most likely GBD's to be found in the structure of these <10$\bar{1}$0> asymmetric tilt boundaries. In the misorientation range 30° < θ < 37.5° GBD's with Burgers vectors $b_p$ = a/15 <22$\bar{4}$3> are to be expected near 30°, $b_p$ = a/23 <22$\bar{4}$1> just below 34.25°, and $b_p$ = a/69 <7 7 $\overline{14}$ 15> above 34.25°. In the misorientation range 49.6° < θ < 56.6°, the most likely pattern-preserving GBD's appear to be $b_p$ = a/51 <44$\bar{8}$3> near 49.6° and $b_p$ = a/9 <22$\bar{4}$3> near 56.6°.

The GBD's of the pattern-preserving array are seen to produce a grain boundary shear which is balanced by an array of misfit dislocations, the pattern-preserving array and the misfit array together accounting for the total dislocation content of the boundary. The strength of the Burgers vector of the misfit array is calculated as a function of misorientation for several of the possible pattern-preserving GBD's.

Various factors which appear to have influenced the selection of the more prevalent pattern-preserving GBD's in these asymmetric <10$\bar{1}$0> tilt boundaries in zinc are discussed. Among them, it appears that the GBD's in these faceted boundaries have a tendency to have core structures equivalent to the structural units in the previous coincidence structural unit model. From this standpoint, the equivalence of the GBD description and the coincidence structural unit model is clearly demonstrated.

# LITERATURE CITED


1. SCHOBER, T., and BALLUFFI, R. W. *Quantitative Observation of Misfit Dislocation Arrays in Low and High-Angle Twist Grain Boundaries.* Phil. Mag., v. 21, 1970, p. 109-123.
2. SCHOBER, T. *Observation of Misfit Dislocation Arrays in High Angle (110) Twist Grain Boundaries in Gold.* Phil. Mag., v. 22, 1970, p. 1063-1068.
3. SCHOBER, T., and BALLUFFI, R. W. *Extraneous Grain Boundary Dislocations in Low and High Angle (001) Twist Boundaries in Gold.* Phil. Mag., v. 24, 1971, p. 165-180.
4. SCHOBER, T., and BALLUFFI, R. W. *Dislocations in Symmetric High Angle [001] Tilt Boundaries in Gold.* Phys. Stat. Sol. (b), v. 44, 1971, p. 115-126.
5. SCHOBER, T., and WARRINGTON, D. H. *Extraneous Grain Boundary Dislocations in High Angle (110) Twist Boundaries in Gold.* Phys. Stat. Sol. (a), v. 6, 1971, p. 103-110.
6. BALLUFFI, R. W., KOMEN, Y., and SCHOBER, T. *Electron Microscope Studies of Grain Boundary Dislocation Behavior.* Surface Science, v. 31, 1972, p. 68-103.
7. BOLLMANN, W. *Crystal Defects and Crystalline Interfaces.* Springer-Verlag, 1970.
8. BALLUFFI, R. W., WOOLHOUSE, G. R., and KOMEN, Y. *On Grain Boundary Dislocation Contrast in the Electron Microscope* in The Nature and Behavior of Grain Boundaries. H. Hu, ed., Plenum Press, 1972, p. 41.
9. BALLUFFI, R. W., and TAN, T. Y. *Comments on the Range of Applicability of the Grain Boundary (Secondary) Dislocation Model to High Angle Grain Boundaries.* Scripta Met., v. 6, 1972, p. 1033-1040.
10. LOBERG, B., and SMITH, D. A. *Periodic Structures and Grain Boundaries in Magnesium.* J. Microscopy, v. 102, 1974, p. 317-322.
11. BRUGGEMAN, G. A., and BISHOP, G. H. *Grain Boundary Dislocations in Noncubic Crystals - I. The Model.* Army Materials and Mechanics Research Center, AMMRC TR 76-6, March 1976.
12. BISHOP, G. H., HARTT, W. H., and BRUGGEMAN, G. A. *Grain Boundary Faceting of $<10\bar{1}0>$ Tilt Boundaries in Zinc.* Acta Met., v. 19, 1971, p. 37-47.
13. HARTT, W. H., BISHOP, G. H., and BRUGGEMAN, G. A. *Grain Boundary Faceting of $<10\bar{1}0>$ Tilt Boundaries in Zinc - Part II.* Acta Met., v. 22, 1974, p. 971-983.
14. BISHOP, G. H., and CHALMERS, B. *A Coincidence-Ledge-Dislocation Description of Grain Boundaries.* Scripta Met., v. 2, 1968, p. 133-140.
15. BISHOP, G. H., and CHALMERS, B. *Dislocation Structure and Contrast in High-Angle Grain Boundaries.* Phil. Mag., v. 24, 1971, p. 515-526.
16. BRUGGEMAN, G. A., BISHOP, G. H., and HARTT, W. H. *Coincidence and Near-Coincidence Grain Boundaries in HCP Metals* in The Nature and Behavior of Grain Boundaries. H. Hu, ed., Plenum Press, 1972, p. 83.
17. HIRTH, J. P., and BALLUFFI, R. W. *On Grain Boundary Dislocations and Ledges.* Acta Met., v. 21, 1973, p. 929-942.

TECHNICAL REPORT DISTRIBUTION

| No. of Copies | To |
|---|---|
| 1 | Office of the Director, Defense Research and Engineering, The Pentagon, Washington, D. C. 20301 |
| 12 | Commander, Defense Documentation Center, Cameron Station, Building 5, 5010 Duke Street, Alexandria, Virginia 22314 |
| 1 | Metals and Ceramics Information Center, Battelle Memorial Institute, 505 King Avenue, Columbus, Ohio 43201 |
| 1 | Chemical Propulsion Information Agency, Applied Physics Laboratory, The Johns Hopkins University, 8621 Georgia Avenue, Silver Spring, Maryland 20910 |
| | Chief of Research and Development, Department of the Army, Washington, D. C. 20310 |
| 2 | ATTN: Physical and Engineering Sciences Division |
| | Commander, Army Research Office, P. O. Box 12211, Research Triangle Park, North Carolina 27709 |
| 1 | ATTN: Information Processing Office |
| | Commander, U. S. Army Materiel Development and Readiness Command, 5001 Eisenhower Avenue, Alexandria, Virginia 22333 |
| 1 | ATTN: DRCDE-TC |
| 1 | DRCSA-S, Dr. R. B. Dillaway, Chief Scientist |
| | Commander, U. S. Army Electronics Command, Fort Monmouth, New Jersey 07703 |
| 1 | ATTN: DRSEL-GG-DD |
| 1 | DRSEL-GG-DM |
| | Commander, U. S. Army Missile Command, Redstone Arsenal, Alabama 35809 |
| 1 | ATTN: Technical Library |
| 1 | DRSMI-RSM, Mr. E. J. Wheelahan |
| | Commander, U. S. Army Armament Command, Rock Island, Illinois 61201 |
| 2 | ATTN: Technical Library |
| | Commander, U. S. Army Natick Laboratories, Natick, Massachusetts 01760 |
| 1 | ATTN: Technical Library |
| | Commander, U. S. Army Satellite Communications Agency, Fort Monmouth, New Jersey 07703 |
| 1 | ATTN: Technical Document Center |
| | Commander, U. S. Army Tank-Automotive Development Center, Warren, Michigan 48090 |
| 2 | ATTN: DRDTA, Research Library Branch |
| | Commander, White Sands Missile Range, New Mexico 88002 |
| 1 | ATTN: STEWS-WS-VT |
| | Commander, Aberdeen Proving Ground, Maryland 21005 |
| 1 | ATTN: STEAP-TL, Bldg. 305 |
| | President, Airborne, Electronics and Special Warfare Board, Fort Bragg, North Carolina 28307 |
| 1 | ATTN: Library |
| | Commander, Dugway Proving Ground, Dugway, Utah 84022 |
| 1 | ATTN: Technical Library, Technical Information Division |
| | Commander, Edgewood Arsenal, Maryland 21010 |
| 1 | ATTN: Mr. F. E. Thompson, Dir. of Eng. & Ind. Serv., Chem-Mun Br |
| | Commander, Frankford Arsenal, Philadelphia, Pennsylvania 19137 |
| 1 | ATTN: Library, H1300, Bl. 51-2 |
| 1 | SMUFA-L300, Mr. J. Corrie |
| | Commander, Harry Diamond Laboratories, 2800 Powder Mill Road, Adelphi, Maryland 20783 |
| 1 | ATTN: Technical Information Office |
| | Commander, Picatinny Arsenal, Dover, New Jersey 07801 |
| 1 | ATTN: SMUPA-RT-S |
| | Commander, Redstone Scientific Information Center, U. S. Army Missile Command, Redstone Arsenal, Alabama 35809 |
| 4 | ATTN: DRSMI-RBLD, Document Section |
| | Commander, Watervliet Arsenal, Watervliet, New York 12189 |
| 1 | ATTN: SARWV-RDT, Technical Information Services Office |
| | Commander, U. S. Army Foreign Science and Technology Center, 220 7th Street, N. E., Charlottesville, Virginia 22901 |
| 1 | ATTN: DRXST-SD3 |
| | Director, Eustis Directorate, U. S. Army Air Mobility Research and Development Laboratory, Fort Eustis, Virginia 23604 |
| 1 | ATTN: Mr. J. Robinson, SAVDL-EU-SS |
| | Librarian, U. S. Army Aviation School Library, Fort Rucker, Alabama 36360 |
| 1 | ATTN: Building 5907 |
| | Commander, U. S. Army Engineer School, Fort Belvoir, Virginia 22060 |
| 1 | ATTN: Library |
| | Commandant, U. S. Army Quartermaster School, Fort Lee, Virginia 23801 |
| 1 | ATTN: Quartermaster School Library |
| | Naval Research Laboratory, Washington, D. C. 20375 |
| 1 | ATTN: Dr. J. M. Krafft - Code 8430 |
| 2 | Dr. G. R. Yoder - Code 6382 |
| | Chief of Naval Research, Arlington, Virginia 22217 |
| 1 | ATTN: Code 471 |
| | Air Force Materials Laboratory, Wright-Patterson Air Force Base, Ohio 45433 |
| 2 | ATTN: AFML (MXE), E. Morrissey |
| 1 | AFML (LC) |
| 1 | AFML (LMD), D. M. Forney |
| 1 | AFML (MBC), S. Schulman |
| | National Aeronautics and Space Administration, Washington, D. C. 20546 |
| 1 | ATTN: Mr. B. G. Achhammer |
| 1 | Mr. G. C. Deutsch - Code RR-1 |
| | National Aeronautics and Space Administration, Marshall Space Flight Center, Huntsville, Alabama 35812 |
| 1 | ATTN: R-P&VE-M, R. J. Schwinghamer |
| 1 | S&E-ME-MM, Mr. W. A. Wilson, Building 4720 |
| 1 | Ship Research Committee, Maritime Transportation Research Board, National Research Council, 2101 Constitution Ave., N. W., Washington, D. C. 20418 |
| | P. R. Mallory Company, Inc., 3029 East Washington Street, Indianapolis, Indiana 46206 |
| 1 | ATTN: Technical Library |
| | Wyman-Gordon Company, Worcester, Massachusetts 01601 |
| 1 | ATTN: Technical Library |
| 1 | The Charles Stark Draper Laboratory, 68 Albany Street, Cambridge, Massachusetts 02139 |
| 1 | Materials Sciences Corporation, Blue Bell Campus, Merion Towle Bldg., Blue Bell, Pennsylvania 19422 |
| | Director, Army Materials and Mechanics Research Center, Watertown, Massachusetts 02172 |
| 2 | ATTN: DRXMR-PL |
| 1 | DRXMR-AG |
| 2 | Authors |

Army Materials and Mechanics Research Center,
Watertown, Massachusetts 02172
GRAIN BOUNDARY DISLOCATIONS IN NONCUBIC CRYSTALS - II. THE GBD MODEL APPLIED IN GRAIN BOUNDARY FACETS IN <10$\bar{1}$0> TILT BOUNDARIES IN ZINC -
Gordon A. Bruggeman and George H. Bishop, Jr.

Technical Report AMMRC TR 76-11, March 1976, 21 pp - illus-tables, D/A Project 1T161102B32A,
AMCMS Code 611102.11.855

AD_____

UNCLASSIFIED
UNLIMITED DISTRIBUTION

Key Words

Grain boundaries
Crystallography
Dislocations

Observations of faceting of <10$\bar{1}$0> tilt grain boundaries in zinc and a coincidence structural unit model were reported in earlier papers. The facet inclinations were found to be monotonic functions of boundary misorientation in certain misorientation ranges. In this paper, the grain boundary dislocation (GBD) model developed earlier is used to describe the structure of these faceted boundaries. The model, which assumes the Burgers vectors of the GBD's to be lattice vectors of the complete-pattern-shift or DSC lattice derived from near-coincidence arrays in hcp crystals, is able to account for the experimentally observed changes in boundary inclination with misorientation. Observed facet morphologies are obtained with only certain GBD's, the core structures of which are shown to be equivalent to the structural units in the previously suggested structural unit model. Thus, the application of the GBD model to more general boundaries in noncubic crystals is illustrated, and thereby, the general equivalence of the GBD and coincidence structural unit models is clearly demonstrated.

Army Materials and Mechanics Research Center,
Watertown, Massachusetts 02172
GRAIN BOUNDARY DISLOCATIONS IN NONCUBIC CRYSTALS - II. THE GBD MODEL APPLIED IN GRAIN BOUNDARY FACETS IN <10$\bar{1}$0> TILT BOUNDARIES IN ZINC -
Gordon A. Bruggeman and George H. Bishop, Jr.

Technical Report AMMRC TR 76-11, March 1976, 21 pp - illus-tables, D/A Project 1T161102B32A,
AMCMS Code 611102.11.855

AD_____

UNCLASSIFIED
UNLIMITED DISTRIBUTION

Key Words

Grain boundaries
Crystallography
Dislocations

Observations of faceting of <10$\bar{1}$0> tilt grain boundaries in zinc and a coincidence structural unit model were reported in earlier papers. The facet inclinations were found to be monotonic functions of boundary misorientation in certain misorientation ranges. In this paper, the grain boundary dislocation (GBD) model developed earlier is used to describe the structure of these faceted boundaries. The model, which assumes the Burgers vectors of the GBD's to be lattice vectors of the complete-pattern-shift or DSC lattice derived from near-coincidence arrays in hcp crystals, is able to account for the experimentally observed changes in boundary inclination with misorientation. Observed facet morphologies are obtained with only certain GBD's, the core structures of which are shown to be equivalent to the structural units in the previously suggested structural unit model. Thus, the application of the GBD model to more general boundaries in noncubic crystals is illustrated, and thereby, the general equivalence of the GBD and coincidence structural unit models is clearly demonstrated.

DEPARTMENT OF THE ARMY
ARMY MATERIALS AND MECHANICS RESEARCH CENTER
Watertown, Massachusetts 02172

OFFICIAL BUSINESS

POSTAGE AND FEES PAID
DEPARTMENT OF THE ARMY
DOD 314

THIRD CLASS MAIL

Commander
U. S. Army Armament Command
ATTN: Technical Library
Rock Island, Illinois 61201